Radiation Monitoring Devices Inc.
44 Hunt Street
Watertown, MA 02472

High Resolution Sensor for Nuclear Waste Characterization

Contract # DE-FG02-04ER84056

Principal Investigator: Mr. Kanai Shah
Contributing Scientists: Mr. William Higgins and Dr. Edgar V. Van Loef

Final Report

Period of Performance: 7/13/04 – 4/12/05

Submitted to:

Denise Clarke
U.S. Department of Energy/ACQ
Chicago Operations Office
9800 South Cass Avenue
Argonne, IL 60439

Table of Contents

The research work in the Phase I project was focused on several areas: (i) doping of $LaBr_3$, (ii) investigation of mixed lanthanum halides and growth of crystals, (iii) evaluation of scintillation properties and (iv) measurement of energy resolution.

A. Doping Considerations for $LaBr_3$ and Related Compounds

Most inorganic scintillators used today are based on insulating host crystals in which luminescent ions or complexes are imbedded. Sometimes the luminescent centers are intrinsic, such as the cerium in CeF_3 or the tungstate complex in lead tungstate ($PbWO_4$), and sometimes they are dopants, such as thallium in NaI:Tl or cerium in LSO:Ce. In these materials, the ionizing radiation initially forms holes in the valence band and electrons in the conduction band, with enough energy being transferred to the electron that it comes to rest many atomic diameters away from its original position. The holes are spatially localized (~1 atomic diameter in size) and diffuse to luminescent centers, placing the center in an ionized state. The ionized center then attracts an electron, placing the center in an electrically neutral but excited state, which de-excites by radiating a scintillation photon. The scintillation properties of the inorganic materials, notably the decay lifetime and the light output, are therefore heavily dependent on the luminescent center. The ideal luminescent ion would have a single, optically active electron when it is in its preferred valence state (to prevent undesirable interactions between electrons), a spin / parity allowed transition (to achieve short decay lifetimes), and an ionic radius similar to that of high-Z ions (to allow doping in dense, high-Z host materials).

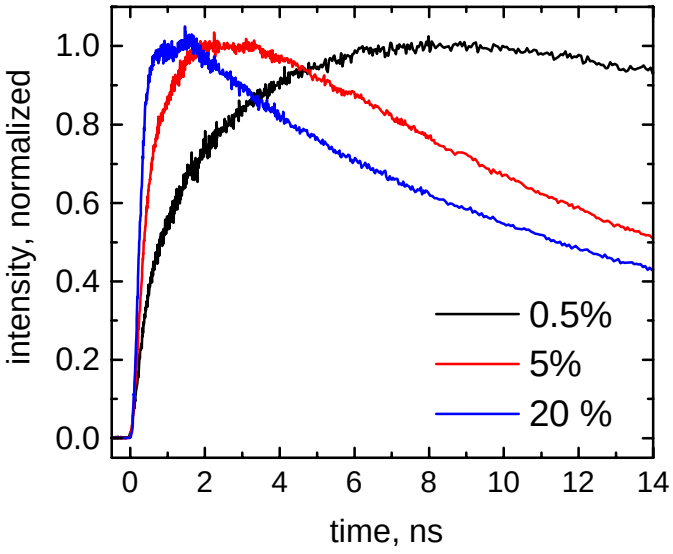

Figure 1. Rise-time spectra for $LaBr_3$ crystals with 0.5, 5, and 20% Ce^{3+} concentrations. The rise-time is faster for samples with higher Ce^{3+} concentration.

Ce^{3+} is a popular dopant for fast, high efficiency luminescence in a number of scintillators such as LSO, GSO, CeF_3 etc. For Ce^{3+} the electric-dipole 5d—4f transition is allowed, and the resultant optical emission is typically bright with 20-40 ns decay time. Ce^{3+} doping has been successfully employed with $LaBr_3$ [Shah 03, van Loef 01a & 01b]. At RMD, we have varied the amount of Ce^{3+} in $LaBr_3$ from 0.5% to 20% (by mole) and have found the rise-time and decay-time to become faster with increasing Ce^{3+} concentration. As an example, the variation of rise-time of $LaBr_3$:Ce samples as a function of Ce^{3+} concentration is shown in **Figure 1**. The light output on the other hand does not change appreciably with varying Ce^{3+} amount [Shah 03, Glodo]. In view of the improvement in timing properties of $LaBr_3$:Ce with higher Ce^{3+} concentration, we also explored $CeBr_3$ in the Phase I research.

We also investigated other dopants (particularly, Eu^{2+} and Pr^{3+}) for $LaBr_3$ in the Phase I project. Eu^{2+} doping has been shown to be promising in other halide scintillators such as CaF_2:Eu^{2+}. The decay time constant of Eu^{2+} luminescence is about 1 μs, which while slower than that of Ce^{3+}, is fast enough to allow high count-rate operation. An attractive feature of Eu^{2+} doping is the possibility of high luminosity. As seen in **Figure 2**, the luminosity of CaF_2:Eu^{2+} is

about two times that of NaI(Tl). As a result, we selected Eu^{2+} as a potential dopant for $LaBr_3$ in the Phase I research. An important requirement in this study was to maintain a reducing atmosphere to prevent Eu^{2+} from changing to Eu^{3+} in the crystal lattice, since Eu^{3+} luminescence is considerably slower and its decay time constant is in the millisecond range.

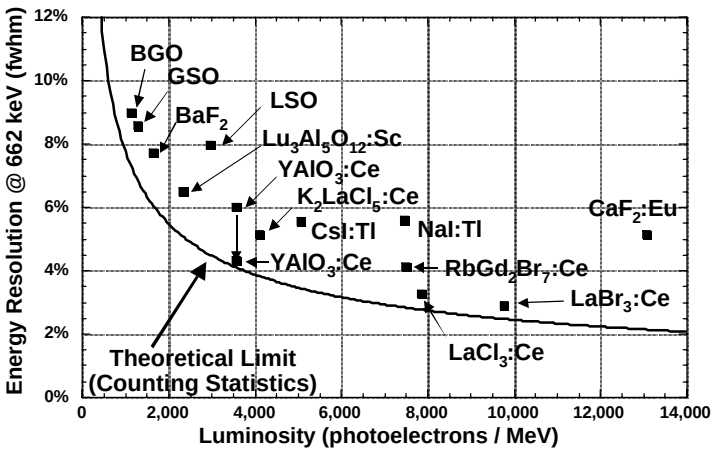

Figure 2: Measured energy resolution of scintillators for 662 keV γ-rays as a function of their light output (expressed as the number of photoelectrons observed with a PMT). The solid curve indicates the theoretical lower limit placed by counting statistics [Moses 2001].

During the Phase I project, we also evaluated Pr^{3+} (praseodymium) as a possible dopant for $LaBr_3$ scintillators. Pr^{3+} doping has been shown to be promising in gadolinium oxysulfide (Gd_2O_2S:Pr or GOS:Pr) [Grabmaier]. Traditionally, GOS has been doped with Tb^{3+}. However, the replacement of Tb^{3+} by Pr^{3+} has provided enhanced performance for GOS screens. This enhancement occurs because in some lattices Pr exhibits a blue-green transition between states of the same multiplicity (^3P_j - ^3H_k), which renders the transition more probable and therefore faster and brighter. It is worth pointing out that Pr^{3+} doping in lanthanum halides has already been successfully tried by other researchers for solid-state infrared laser applications [Bowman], and as a result the compatibility of Pr^{3+} with lanthanum halide crystals has already been verified.

Thus, in addition to Ce^{3+} doping, Eu^{2+} and Pr^{3+} doping of $LaBr_3$ was investigated in the Phase I research.

B. Growth of $LaBr_3$ and Mixed Halide Crystals using Bridgman Method

$LaBr_3$ crystals have hexagonal (UCl_3 type) structure with *P63/m* space group and the density of $LaBr_3$ is 5.3 g/cm^3 [van Loef 01a]. The compound melts congruently at 783 °C and therefore, is well suited for melt based growth methods such as Bridgman and Czochralski processes [Brice]. This is fortunate because these melt-based processes are ideal for growth of large volume crystals [Brice]. During the Phase I project we used Bridgman method (shown in **Figure 3**) for growing $LaBr_3$ crystals because this technique is easy to implement, and can provide good indication of the feasibility of

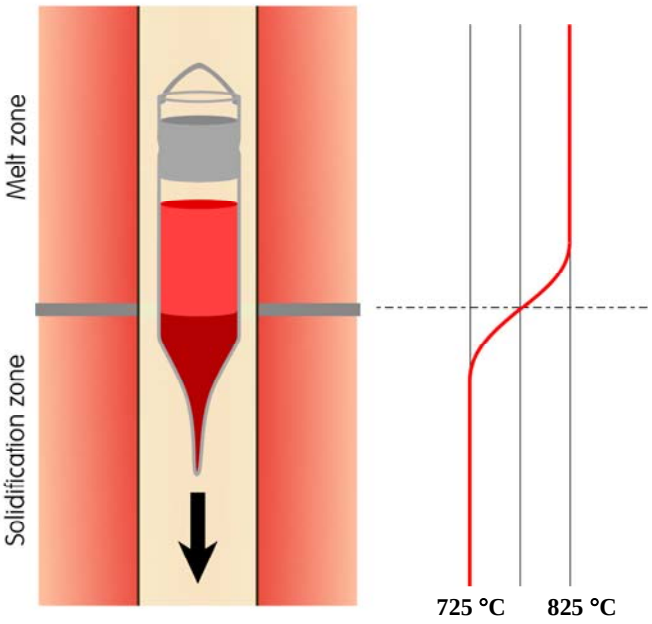

Figure 3. Schematic representation of the Bridgman setup used for La halide growth in the Phase I project.

producing large crystals of $LaBr_3$ from the melt. In fact, many of the commercially available scintillators such as NaI(Tl) and CsI(Tl) are grown using melt based Bridgman and Czochralski techniques. At RMD, we have considerable experience in growing various semiconductors and scintillators using Bridgman technique.

Figure 3 shows a schematic representation of the Bridgman crystal growth process. As shown in the figure, the material to be grown is placed in a crucible inside a two zone furnace and the crucible is slowly dropped through the furnace. The upper furnace zone is kept above the melting point of the compound, and the lower zone is maintained below the melting point. Thus, the feed material in the crucible would melt in the upper zone and crystallize out as the crucible enters the lower zone. This solidification process would be gradual and start from the tip of the crucible, with the melt-solid interface shifting upward (along the length of the crucible) as the crucible is dropped more. The speed at which the crucible is dropped, the temperature gradient in the furnace, and the shape of crucible are important parameters that need to be carefully controlled to grow high quality crystals.

The first step in preparation of $LaBr_3$ crystals was synthesis of $LaBr_3$ doped with desired activators such as Ce^{3+}, Pr^{3+}, and Eu^{2+}. This involved mixing of appropriate amounts of ultra-dry $LaBr_3$ with $CeBr_3$, $PrBr_3$, or $EuBr_2$. These materials were loaded in a quartz ampoule and melted in furnace to allow proper mixing. In case of Eu^{2+} doping reducing environment was employed. Upon cooling, lanthanum bromide doped with desired activator was available. During Bridgman growth, this material was placed in a quartz ampoule and dropped through a two zone furnace (similar to that shown in **Figure 3**) to produce $LaBr_3$ crystals. The growth process involved a controlled solidification of the material along a well established solid-liquid interface (at junction of two furnace zones). Growth rate of ~5 mm/day provided good results for preparation of $LaBr_3$ and was therefore used in the Phase I project. In a related effort, we have now produced $LaBr_3$:Ce crystals that are up to 1" in diameter and 1" long. **Figure 4** shows a photograph of such a $LaBr_3$:Ce crystal grown using Bridgman method.

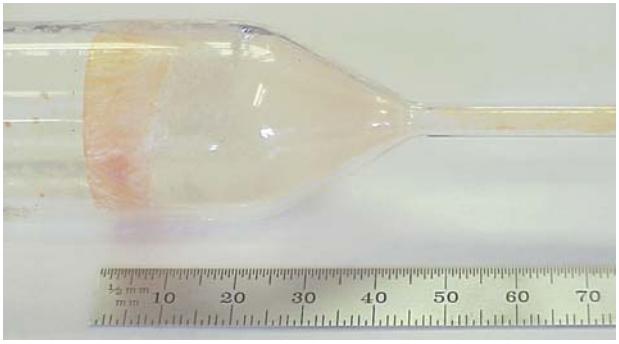

Figure 4. Photograph of a $LaBr_3$:Ce (1" diameter, 1" long) crystal grown at RMD using the Bridgman method.

In addition to growth of $LaBr_3$ with 0.5% Ce^{3+}, 1% Eu^{2+} and 1% Pr^{3+} doping (on molar basis), we also explored growth of related compounds such as $CeBr_3$, $LaBr_{2.4}I_{0.6}$ (with 0.5% Ce doping) and $LaBr_{1.5}Cl_{1.5}$ (with 10% Ce doping). It is worth pointing out that all these compositions have same crystal structure (hexagonal, UCl_3 type) as $LaBr_3$. The temperature settings in the furnace were modified slightly to account for differences in the melting points of the various compositions. Quartz ampoules were used as crucibles in all cases.

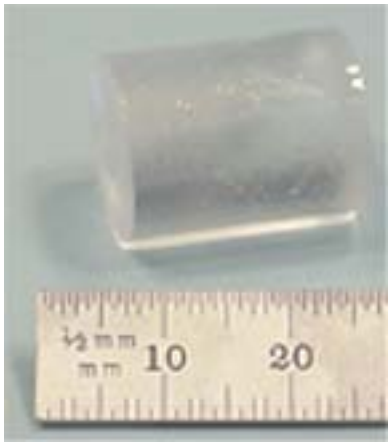

Figure 5. Photograph of $LaBr_3$:Ce crystal (16 mm diameter, 2 cm long), prepared at RMD.

The crystals of all these materials were taken out of their

quartz ampoules and cut using a diamond coated wire saw. The surfaces exposed as a result of these cuts were polished using non-aqueous slurries (due to hygroscopic nature of these materials) prepared by mixing mineral oil with SiO_2, CeO, or Al_2O_3 (< 1 μm grit size). **Figure 5** shows a photograph of a 16 mm diameter $LaBr_3$:Ce crystal (20 mm long) that was prepared in this manner.

The crystals were then packaged to prevent long exposure to moisture. We have begun to explore a new packaging scheme in our research, in which a metal can with two open faces is fabricated. A quartz window (<1 mm thick) is sealed on one open face of the metal can. A scintillation crystal is then placed inside the can and attached to the quartz window using optical epoxy. SiO_2 powder is then packed in the open space between the crystal and the metal can in such a way that all faces of the scintillation crystal except the one attached to the quartz window are completely covered with SiO_2. The top of the metal can is then sealed to a metal disk using epoxy. We have explored this packaging scheme using a $LaBr_3$:Ce crystal (see **Figure 6**) and the results have been promising. Comparison of the light output of the crystal before and after packaging showed that <5% light loss was observed upon packaging. Same approach was used to package other crystal specimens in the Phase I project. Evaluation of scintillation properties of these crystals was then carried out. Results are discussed first for $LaBr_3$:Ce and $CeBr_3$ followed by a discussion of $LaBr_xCl_{3-x}$:Ce and $LaBr_xI_{3-x}$:Ce. Finally, evaluation of $LaBr_3$ doped with Eu^{2+} and Pr^{3+} is discussed.

Figure 6. Photograph of a packaged $LaBr_3$ scintillator.

C. INVESTIGATION OF $LaBr_3$:Ce AND $CeBr_3$

1. Overview

We have evaluated two compositions of the $La_xCe_{1-x}Br$ scintillation family in the Phase I research. This included $LaBr_3$ with 0.5% Ce (with x = 0.995) and $CeBr_3$ (with x = 0). $LaBr_3$ and $CeBr_3$ have hexagonal crystal structure (similar to UCl_3) and their density is 5.3 and 5.2 g/cm^3, respectively. Both these compositions rely on Ce^{3+} ions for luminescence. In case of $LaBr_3$ with 0.5% Ce, cerium is intentionally added as a dopant to provide luminescence, while in case of $CeBr_3$, cerium is an intrinsic constituent as well as an activator. The scintillation properties of $LaBr_3$:Ce (with 0.5% Ce, ~1 cm^3 size or larger) and $CeBr_3$ crystals (<1 cm^3 size) have been investigated at RMD in the Phase I research and the results are discussed here.

2. Emission Spectrum

We have measured the emission spectra of $LaBr_3$:Ce and $CeBr_3$

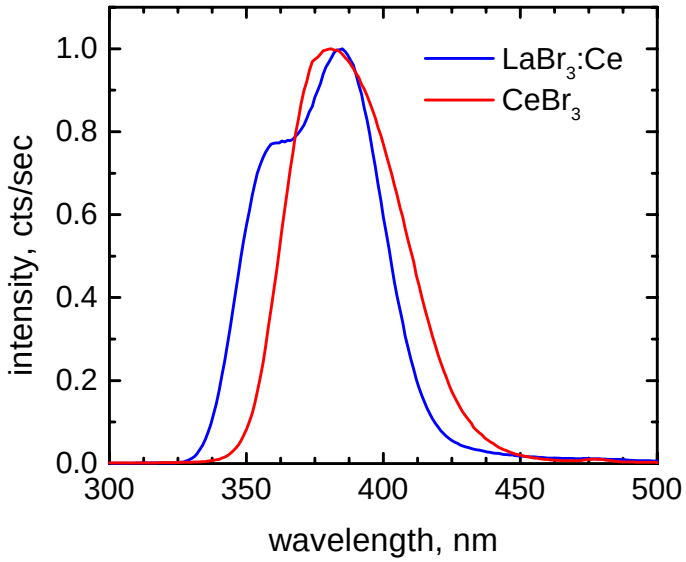

Figure 7. Optical emission spectra of $LaBr_3$:Ce and $CeBr_3$ scintillators upon exposure to X-rays.

scintillators. These samples were excited with X-rays from a Philips tube having a Cu target, with power settings of 30 kVp and 15 mA. The scintillation light was passed through a McPherson monochromator and detected by a Hamamatsu R2059 photomultiplier tube with a quartz window. The system was calibrated with a standard light source to enable correction for sensitivity variations as a function of wavelength. Normalized emission spectra for $LaBr_3$:Ce and $CeBr_3$ samples are shown in **Figure 7**. The peak emission wavelength for both samples is at ~380 nm, which is due to *5d→4f* transition of Ce^{3+}.

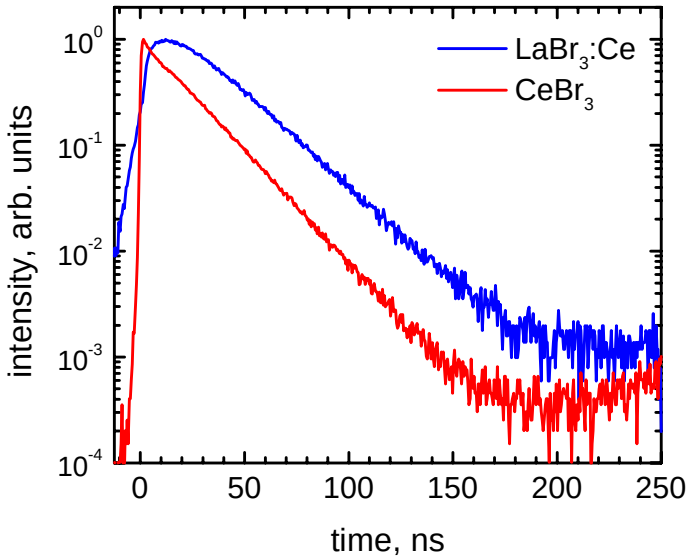

Figure 8. Decay-time spectra for $LaBr_3$:Ce and $CeBr_3$ scintillators.

3. Timing Properties

Decay-time spectra of $LaBr_3$:Ce and $CeBr_3$ crystals have been measured at RMD using the delayed coincidence method [Bollinger]. **Figure 8** shows the decay-time spectra recorded for $LaBr_3$:Ce and $CeBr_3$ samples. From multi-exponential fits to these plots, the principal decay constant for $CeBr_3$ and $LaBr_3$:Ce was estimated to be 17 ns and 26 ns, respectively. The fast decay component in both materials can be attributed to optical emission arising from direct capture of electron-hole pairs at the Ce^{3+} sites. The *initial photon intensity* – a figure of merit for timing applications is estimated to be 2500 and 4000 photons/(ns-MeV) for $LaBr_3$:Ce and $CeBr_3$, respectively. The estimate for $CeBr_3$ is higher compared to all common inorganic scintillators including BaF_2, a benchmark for timing applications.

Coincidence timing resolution of $LaBr_3$:Ce (0.5% Ce) and $CeBr_3$ crystals has been measured at LBNL using the setup shown in **Figure 9**. This experiment involved irradiating BaF_2 and $LaBr_3$:Ce (or $CeBr_3$) scintillators, each coupled to a fast PMT (Hamamatsu R-5320, operated at –2000V) with 511 keV positron annihilation γ-ray pairs (emitted by a ^{68}Ge source). The BaF_2-PMT detector formed a "start" channel in the timing circuit, while the $LaBr_3$ (or $CeBr_3$)-PMT detector formed the "stop" channel. The signal

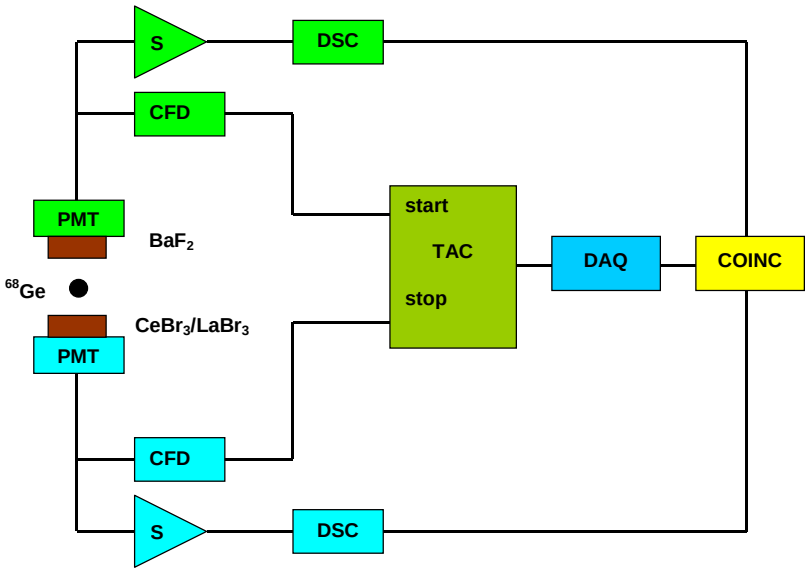

Figure 9. Schematic diagram of setup used to measure coincidence timing resolution of $LaBr_3$/$CeBr_3$ scintillators in Phase I project.

from each detector was processed using two channels of a Tennelec TC-454 CFD that had been modified for use with fast (sub-ns) rise-time PMTs. The time difference between the start and stop signals was digitized with a Tennelec TC-862 TAC and a 16-bit ADC, resulting in a TDC with 7.5 ps per bin resolution. Data were accumulated until the coincidence timing distribution had approximately 10,000 counts in the maximum bin.

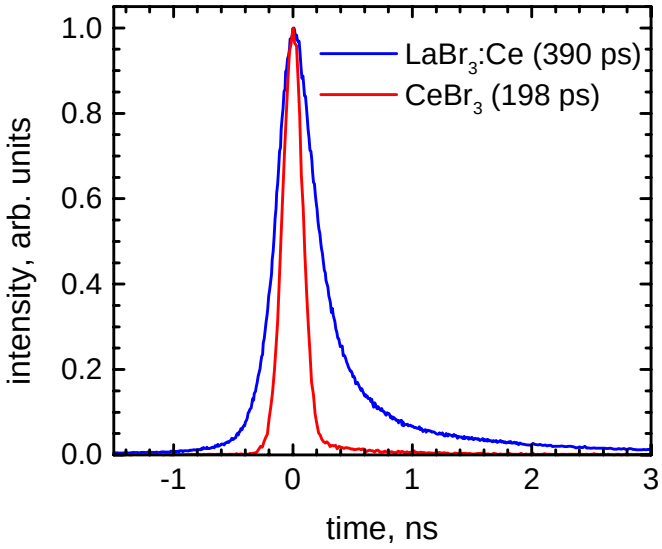

Figure 10. Timing resolution of $LaBr_3$ (0.5% Ce) and $CeBr_3$ crystals in coincidence with BaF_2 upon irradiation with 511 keV gamma-ray pairs.

Figure 10 shows coincidence timing resolution plots acquired at room temperature in this manner with $LaBr_3$:Ce (0.5% Ce) and $CeBr_3$ crystals that were placed in "stop" channel of the timing circuit. (with BaF_2 in the "start" channel in all cases), and the coincidence timing resolution was measured to be 390 ps and 198 ps (FWHM), respectively at room temperature. These results indicate that $LaBr_3$:Ce and $CeBr_3$ scintillators provide excellent timing resolution and they would be suitable for time-of-flight (TOF) studies. It should be noted that the timing resolution of $LaBr_3$:Ce improves substantially as its cerium concentration is increased [Shah 03, Glodo].

4. Light Output and Energy Resolution

Light output (or luminosity) of $LaBr_3$:Ce and $CeBr_3$ crystals have been measured at RMD. $LaBr_3$:Ce and $CeBr_3$ crystals were wrapped with a Teflon tape, coupled to a PMT and then irradiated with 662 keV photons (^{137}Cs source) to record pulse height spectra using standard NIM electronics. A similar experiment was then performed with a calibrated BGO crystal under the same operating conditions. Comparison of the 662 keV gamma-ray peak position recorded with $LaBr_3$:Ce, $CeBr_3$ and BGO scintillators (see **Figure 11**) provided an estimate of the light output of $LaBr_3$:Ce and $CeBr_3$. Amplifier integration time of 4 μs was used.

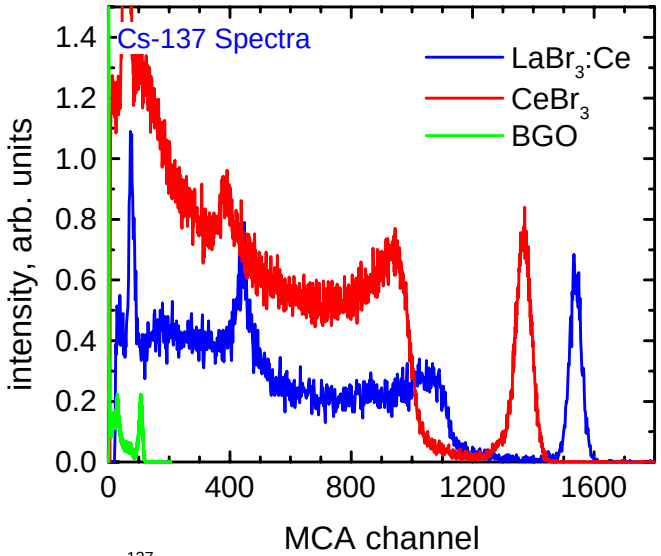

Figure 11. ^{137}Cs spectra collected with $LaBr_3$:Ce, $CeBr_3$ and BGO crystals coupled to PMT. The energy resolution of 662 keV peak for $LaBr_3$:Ce and $CeBr_3$ is ≤3% (FWHM).

The light output of $LaBr_3$:Ce and $CeBr_3$ was found to be ~74,000 and ~68,000 photons/MeV, respectively. This light yield is about 80% higher compared to that of NaI:Tl, and is

among the highest values reported for inorganic scintillators. The theoretical maximum light output of ionic crystals such as $LaBr_3$:Ce and $CeBr_3$ can be estimated to be as high as 125,000 photons/MeV (based on their bandgap). Thus, further improvement in light output should be possible upon optimization of these crystals.

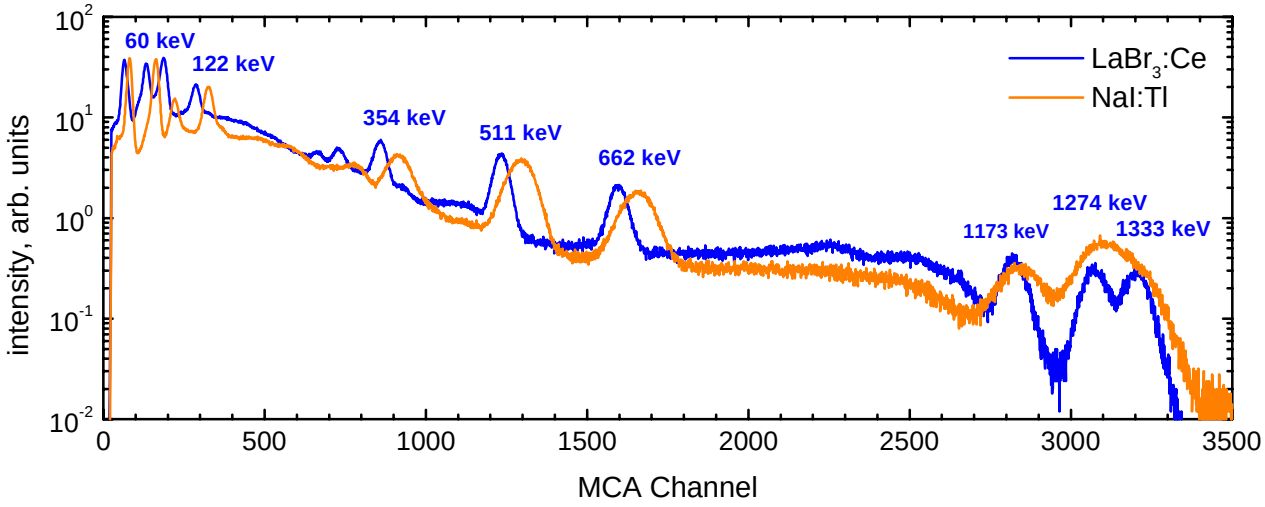

Figure 12 Energy spectra recorded with NaI:Tl and $LaBr_3$:Ce scintillators (coupled to PMT) upon exposure to multiple gamma-ray sources (^{241}Am, ^{57}Co, ^{133}Ba, ^{22}Na, ^{137}Cs, and ^{60}Co). Superior energy resolution of $LaBr_3$:Ce is clearly visible in the figure.

$LaBr_3$:Ce and $CeBr_3$ show excellent energy resolution. As shown in **Figure 11**, energy resolution of ~3% (FWHM) or less has been recorded with $LaBr_3$:Ce and $CeBr_3$ crystals for 662 keV γ-rays (^{137}Cs source) with the scintillators coupled to a PMT. Such high resolution has never been achieved before with any of the established scintillation materials (such as NaI:Tl, CsI:Tl, LSO, BGO, and GSO) even in form of small crystals. The energy resolution of $LaBr_3$:Ce and $CeBr_3$ at 662 keV γ-energy is almost twice as good as that for NaI:Tl. This is illustrated in energy spectra recorded with $LaBr_3$:Ce and NaI:Tl crystals coupled to a PMT (see **Figure 12**) upon exposure to multiple radiation sources such as ^{241}Am (60 keV photons), ^{57}Co (122 keV photons), ^{133}Ba (354 keV photons), ^{22}Na (511 keV and 1274 keV photons), ^{137}Cs (662 keV photons) and ^{60}Co (1173 and 1333 keV photons). $LaBr_3$:Ce crystal used in this study was 1" long. The superior energy resolution of $LaBr_3$:Ce is clearly observed in the spectra. For example, the NaI:Tl detector is not able to separate the 1274 keV and 1333 keV gamma-ray emissions, while these gamma-lines are well-resolved in the spectrum recorded with $LaBr_3$:Ce detector. Similarly, various features near the 354 keV peak (^{133}Ba source) are well-resolved with $LaBr_3$:Ce detector, which is not the case with NaI:Tl detector. Furthermore, the peaks corresponding to 354, 511, 662 and 1173 keV gamma-ray energies are much broader in the spectrum recorded with NaI:Tl compared to that for $LaBr_3$:Ce, confirming the superior energy resolution of the $LaBr_3$:Ce detector. Similar performance is expected from $CeBr_3$ crystals.

5. Proportionality

We have evaluated the proportionality of response of $LaBr_3$:Ce and $CeBr_3$ scintillators. Non-proportionality (as a function of energy) in light yield is one of the important reasons behind the degradation in energy resolution of established scintillators such as NaI:Tl and LSO [Moses]. We have measured light output of $LaBr_3$:Ce and $CeBr_3$ under excitation from isotopes

such as ^{57}Co (122 keV γ-rays), ^{22}Na (511 keV and 1274 keV γ-rays), ^{133}Ba (354 keV γ-rays), and ^{137}Cs (662 keV γ-rays). From the measured peak position and the known γ-ray energy for each isotope, the light output (in photons/MeV) at each γ-ray energy was estimated. The data points were then normalized with respect to the light output value at 662 keV energy and the results indicate that $CeBr_3$ and $LaBr_3$:Ce are fairly proportional scintillators. As shown in **Figure 13**, over the measured energy range (100 keV to 1300 keV), the non-proportionality in light yield is about 5% for $CeBr_3$ and 2% for $LaBr_3$:Ce, which is substantially better than that for many established scintillators. Over the same energy range, the non-proportionality is about 35% for LSO and about 20% for NaI:Tl and CsI:Tl [Guillot-Noel]. Good proportionality in combination with high light output explains high energy resolution of $LaBr_3$:Ce and $CeBr_3$ and we believe that further improvement in energy resolution should be possible as crystals with better optical quality and uniformity are produced.

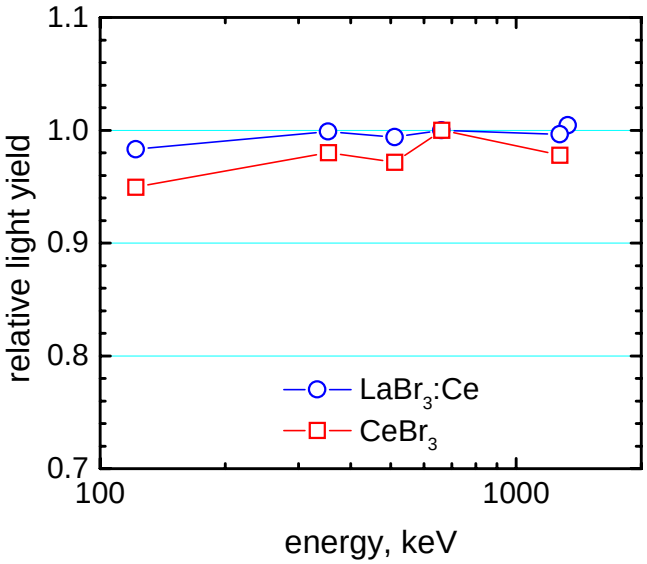

Figure 13. Proportionality of response as a function of gamma-ray energy for $LaBr_3$:Ce and $CeBr_3$ crystals.

In the Phase I effort, we have also confirmed that large crystals of $LaBr_3$:Ce provide excellent energy resolution. For example, using a 16 mm diameter, 2 cm long $LaBr_3$:Ce crystal (shown earlier in **Figure 5**) coupled to a PMT, ^{137}Cs spectrum was acquired (see **Figure 14**). The resolution of the 662 keV gamma-ray peak was measured to be ~3.5% (FWHM) at room temperature, which is very impressive. These results confirm the potential of these new scintillators in gamma-ray spectroscopy.

6. Comparison of $CeBr_3$ and $LaBr_3$:Ce

Overall, these characteristics clearly indicate that $LaBr_3$:Ce and $CeBr_3$ are very promising scintillators and they should be well suited as gamma ray detectors for monitoring of nuclear materials. Our measurements indicated that physical and scintillation properties of $CeBr_3$ and $LaBr_3$:Ce are very similar. The dominant luminescence in both scintillators is due to Ce^{3+}. In case of $LaBr_3$:Ce, cerium is a dopant and it is intentionally added to enhance the scintillation performance of the material. In case of $CeBr_3$, cerium is an intrinsic constituent as well as an activator for the luminescence process, which simplifies material preparation and maintaining Ce^{3+}

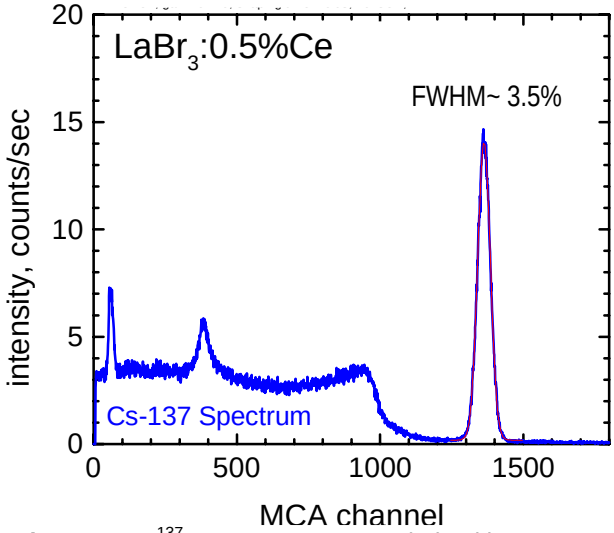

Figure 14. ^{137}Cs spectrum recorded with a $LaBr_3$ crystal (16 mm diameter, 2 cm long) coupled to a PMT with 3.5% FWHM resolution for 662 keV peak.

uniformity in large crystals. One issue that differentiates $CeBr_3$ and $LaBr_3$ is their self-activity due to presence of radioactive isotopes. In $LaBr_3$, self-activity is primarily due to ^{138}La that emits conversion electrons and β-particles with energy of up to 1.7 MeV. The self-activity due to ^{138}La in $LaBr_3$ has an intrinsic count-rate of ~1.5 events/(cm^3•sec). The self-activity of $CeBr_3$ (due to ^{142}Ce that emits β-particles with total energy of 4.5 MeV) is $4x10^{-4}$ events/(cm^3•sec). Thus, the self-activity of $CeBr_3$ is about 3750 times lower than that in $LaBr_3$. Such negligible self-activity of $CeBr_3$ makes it much more attractive in some applications where large detector volumes are required and the expected extrinsic count-rate is very low.

Overall, both materials are promising and we will continue to investigate them in parallel in the Phase II effort. The scintillation properties of $LaBr_3$ (with 0.5% Ce) and $CeBr_3$ along with those for other crystal compositions investigated in Phase I research are summarized in **Table 1** at the end of this final report. Scintillation properties of $LaBr_xCl_{3-x}$:Ce and $LaBr_xI_{3-x}$:Ce crystals were also measured in the Phase I project as discussed in the following section.

D. Investigation of $LaBr_xCl_{3-x}$:Ce and $LaBr_xI_{3-x}$:Ce

During the Phase I project, we have also investigated mixed lanthanum halide compositions, $LaBr_xCl_{3-x}$ and $LaBr_xI_{3-x}$, which were doped with cerium. The motivation behind this study was to vary the bandgap of the compositions and investigate the effect on the scintillation performance. Furthermore, in some instances (for example, $Cd_xZn_{1-x}Te$ or CZT) the ternary mixtures provide increased flexibility in the crystal lattice and thereby, allow easier growth of larger crystals. Based on our prior experience with the binary compounds, $LaCl_3$, $LaBr_3$, and LaI_3, and their crystal structures, we selected following two compositions for our investigation: $LaBr_{2.4}I_{0.6}$ (with 0.5% Ce doping) and $LaBr_{1.5}Cl_{1.5}$ (with 10% Ce doping). The doping level of 0.5% Ce was chosen for $LaBr_{2.4}I_{0.6}$ because this doping level is sufficient for both $LaBr_3$ and LaI_3. In case of $LaBr_{1.5}Cl_{1.5}$, 10% Ce level was chosen because $LaCl_3$ requires 10% Ce for optimal performance [van Loef 00]. Light output, energy resolution, proportionality, and emission and decay spectra were measured for $LaBr_{2.4}I_{0.6}$:Ce and $LaBr_{1.5}Cl_{1.5}$:Ce crystals (<1 cm^3 size) in the Phase I project.

1. Light Output and Energy Resolution Measurements

Light output of $LaBr_{2.4}I_{0.6}$:Ce and $LaBr_{1.5}Cl_{1.5}$:Ce crystals was measured in similar manner as that described earlier for $LaBr_3$:Ce and $CeBr_3$ crystals and involved recording ^{137}Cs spectra (see **Figure 15**) with these scintillators (wrapped with Teflon) coupled to a PMT. ^{137}Cs spectrum with a calibrated BGO crystal (with known light output of 8000 photons/MeV) was also recorded for comparison. From comparison of the 662 keV gamma-ray peak position for BGO, $LaBr_{2.4}I_{0.6}$:Ce and $LaBr_{1.5}Cl_{1.5}$:Ce crystals, the light output of $LaBr_{2.4}I_{0.6}$ (with 0.5% Ce) and $LaBr_{1.5}Cl_{1.5}$ (with 10% Ce)

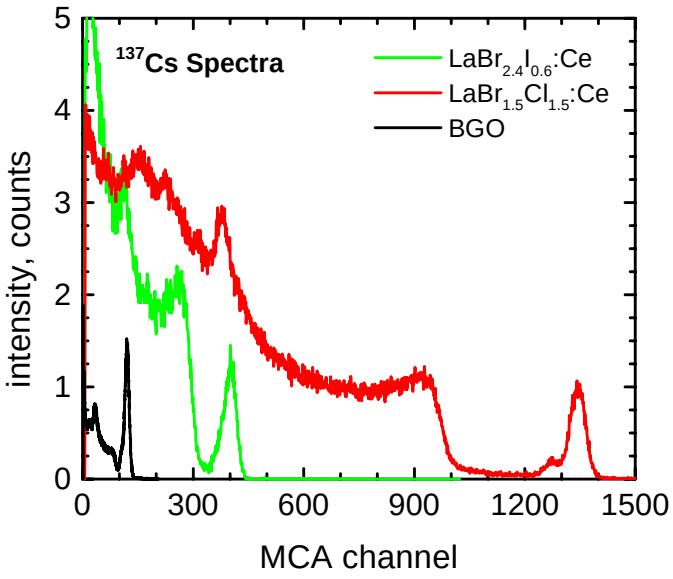

Figure 15. ^{137}Cs spectra collected with $LaBr_{1.5}Cl_{1.5}$ (with 10% Ce), $LaBr_{2.4}I_{0.6}$ (with 0.5% Ce) and BGO.

was estimated to be ~30,000 photons/MeV and ~68,000 photons/MeV, respectively. While the light output of $LaBr_{2.4}I_{0.6}$:Ce is lower compared to $LaBr_3$:Ce, the light output of $LaBr_{1.5}Cl_{1.5}$:Ce is excellent and is similar to that for $LaBr_3$:Ce and $CeBr_3$.

Gamma ray energy resolution of $LaBr_{2.4}I_{0.6}$:Ce and $LaBr_{1.5}Cl_{1.5}$:Ce crystals was also estimated from the energy spectra shown in **Figure 15**. The 662 keV energy resolution of $LaBr_{2.4}I_{0.6}$:Ce crystal is ~7% (FWHM) using a double Gaussian fit, while that of $LaBr_{1.5}Cl_{1.5}$:Ce is excellent (<3.5% FWHM), which is very encouraging. $LaBr_{1.5}Cl_{1.5}$ (10% Ce) also shows good proportionality. Over 100 keV to >1 MeV gamma-ray energy range, its non-proportionality is ~5%. Based on the light output and energy resolution studies, $LaBr_{1.5}Cl_{1.5}$:Ce appears to be a promising scintillator for γ-ray spectroscopy.

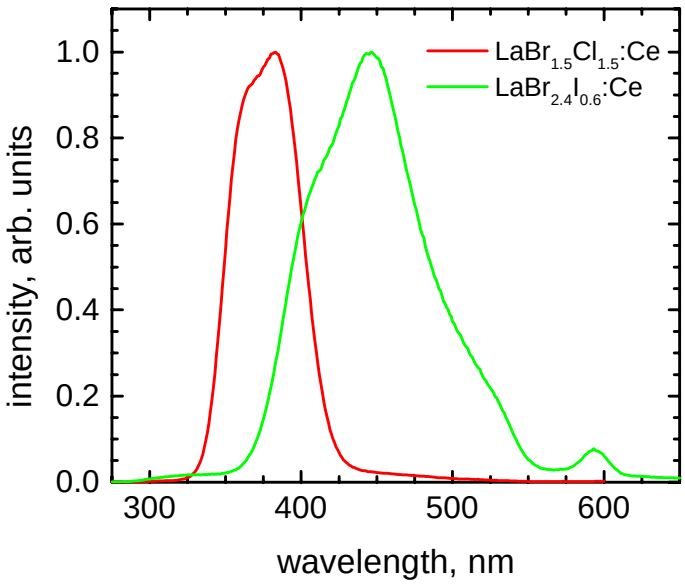

Figure 16. X-ray excited emission spectra for $LaBr_{1.5}Cl_{1.5}$ (with 10% Ce) and $LaBr_{2.4}I_{0.6}$ (with 0.5% Ce).

2. Emission Spectra

During the Phase I program we measured emission spectra of $LaBr_{2.4}I_{0.6}$:Ce and $LaBr_{1.5}Cl_{1.5}$:Ce crystals. During these measurements, good quality crystals were covered on all sides (except the polished front face) with a reflective Teflon tape. The samples were excited with a Philips X-ray tube having a copper target, with power settings of 30 kVp and 15 mA. The scintillation light was passed through a McPherson monochromator and detected by a Hamamatsu R2059 photomultiplier tube with a quartz window. This data was corrected by taking into account the spectral response of the PMT and a background subtraction was also performed. **Figure 16** shows the emission spectra for $LaBr_{2.4}I_{0.6}$:Ce and $LaBr_{1.5}Cl_{1.5}$:Ce crystals measured in this manner. The peak emission wavelength for $LaBr_{1.5}Cl_{1.5}$:Ce is ~380 nm which is similar to that for $LaBr_3$:Ce and $CeBr_3$ crystals while that of $LaBr_{2.4}I_{0.6}$:Ce is ~450 nm. The emission peak in both cases is due to $5d \rightarrow 4f$ transition of Ce^{3+}.

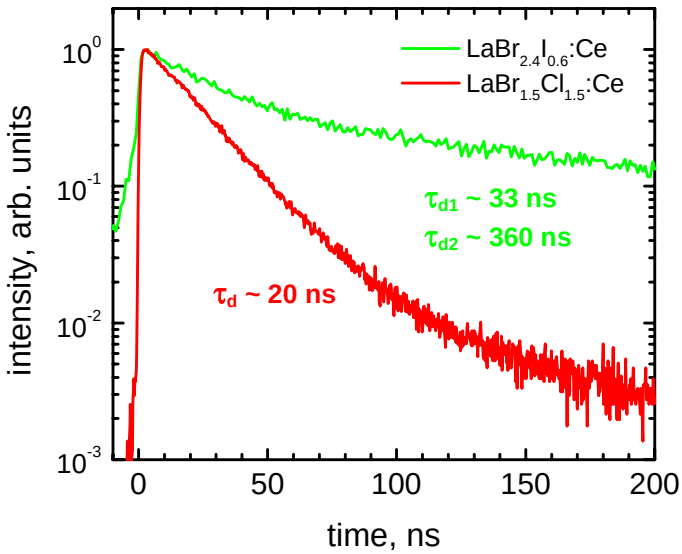

Figure 17. Decay time spectra for $LaBr_{1.5}Cl_{1.5}$ (with 10% Ce) and $LaBr_{2.4}I_{0.6}$ (with 0.5% Ce).

3. Decay time Spectra

Decay-time spectra of $LaBr_{2.4}I_{0.6}$:Ce and $LaBr_{1.5}Cl_{1.5}$:Ce crystals upon irradiation with 662 keV gamma-rays (^{137}Cs source) have been measured at RMD using the delayed coincidence method [Bollinger]. **Figure 17** shows the resulting decay-time plots for these crystals. By fitting the data to an exponentially decaying lifetime model, decay components were estimated for these crystals. The principal decay time constant for $LaBr_{1.5}Cl_{1.5}$ (10% Ce) was ~20 ns and this component covered almost all of the light emitted. In case of $LaBr_{2.4}I_{0.6}$ (0.5% Ce), two decay components with 33 ns and 360 ns time constants were present. Thus, $LaBr_{1.5}Cl_{1.5}$ (10% Ce) shows faster response.

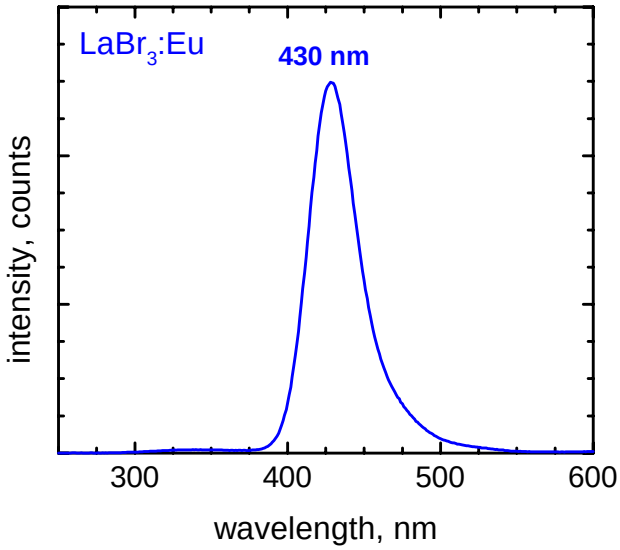

Figure 18. X-ray induced emission spectrum of $LaBr_3$ doped with 1% Eu^{2+} (on molar basis).

Timing resolution of $LaBr_{1.5}Cl_{1.5}$ (10% Ce) in coincidence with BaF_2 was measured to be 220 ps (FWHM) upon exposure to 511 keV gamma-ray pairs by Dr. Moses at LBNL using the setup shown earlier in **Figure 9**. Thus, $LaBr_{1.5}Cl_{1.5}$ (10% Ce) is an excellent scintillator with properties matching those for $LaBr_3$:Ce and $CeBr_3$. The scintillation properties of $LaBr_{2.4}I_{0.6}$ (0.5% Ce) and $LaBr_{1.5}Cl_{1.5}$ (10% Ce) crystals along with those for other crystal compositions investigated in the Phase I research are summarized in **Table 1** at the end of this final report. Properties of $LaBr_3$:Eu^{2+} crystals are discussed in the following section.

E. Investigation of Eu^{2+} Doped $LaBr_3$

During the Phase I research, we have investigated crystals of lanthanum bromide doped with Eu^{2+} in place of Ce^{3+} as scintillators. The motivation behind this study was to investigate the luminescence produced by Eu^{2+} in $LaBr_3$ host crystals because Eu^{2+} is also a very efficient activator and in some host specimens (for example, CaF_2) it provides very bright luminescence. During the Phase I research, we produced crystals of $LaBr_3$ doped with 1% Eu^{2+} (on molar basis) and studied scintillation properties such as emission spectrum, decay time spectrum and light output of the specimens. These measurements were performed in similar manner as that described in earlier sections.

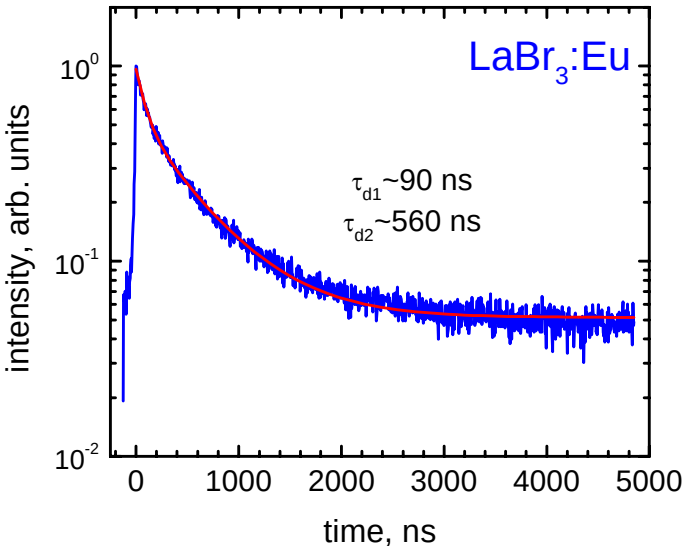

Figure 19. Gamma ray induced decay time spectrum of a $LaBr_3$:Eu^{2+} sample.

Figure 18 shows an X-ray induced emission spectrum of a $LaBr_3$ sample doped with 1% Eu^{2+}, which shows a well defined band peaking at 430 nm. This wavelength is typical for Eu^{2+} doped materials [Dorenbos 03]. For example, maximum of emission in CaF_2:Eu^{2+} is around 425 nm. This emission, as in case of Ce^{3+}, is due to *d-f* transitions of Eu^{2+}.

The decay time spectrum of $LaBr_3$:Eu^{2+} has been measured upon exposure to 662 keV gamma-rays (^{137}Cs source) using the delayed coincidence method [Bollinger] and the resulting temporal response is shown in **Figure 19**. While the fastest decay component is ~90 ns in this case, the principal decay time constant is ~560 ns. It should be noted that the temporal response covering these two components decays over only 1-2 orders of magnitude from the peak value, which suggests that slower components are also present. This was confirmed by performing afterglow measurements on $LaBr_3$:Eu^{2+} samples.

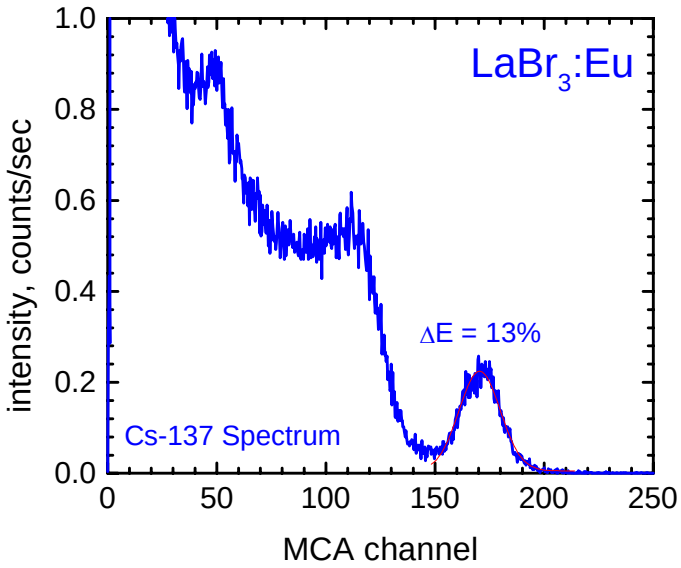

Figure 20. ^{137}Cs spectrum with a $LaBr_3$ crystal doped with 1% Eu^{2+}. Based on prior calibration with BGO crystal, the light output of $LaBr_3$:Eu was estimated to be 10,000 photons/MeV and its energy resolution was 13% (FWHM).

Finally, light output of $LaBr_3$:Eu^{2+} sample has also been measured in the Phase I project. The experiment involved recording a 662 keV gamma-ray spectrum with a $LaBr_3$:Eu^{2+} crystal (wrapped in Teflon) which is shown in **Figure 20**. Based on previous calibration of the energy scale with a BGO sample, the light output of $LaBr_3$ (1% Eu^{2+}) was estimated to be ~10,000 photons/MeV. This low light output can be explained on the basis of slow components (>50 μs) that are present in $LaBr_3$:Eu^{2+}. Since the light emitted by the slow components falls outside the integration window (up to 12 μs) of spectroscopy amplifier, it is not included in the light estimation. The energy resolution of the 662 keV photopeak was measured to be 13% (FWHM) in this case.

Our hypothesis regarding the slow components in $LaBr_3$:Eu^{2+} is that they are caused by presence of charge traps in the crystals. One possible cause of such traps could be the charge imbalance caused upon Eu^{2+} ions replacing the La^{3+} ions in the host lattice. Such defects can be removed by co-doping the crystal with ions (such as Hf^{4+}) that restore charge neutrality, which will be the focus of a future research effort. The scintillation properties of $LaBr_3$:Eu^{2+} crystals along with those for other crystal compositions investigated in the Phase I research are summarized in **Table 1** at the end of this final report. Scintillation properties of $LaBr_3$:Pr^{3+} crystals were also measured in the Phase I project as discussed in the following section.

F. INVESTIGATION OF $LaBr_3$ DOPED WITH Pr^{3+}

During the Phase I research, we have also investigated crystals of lanthanum bromide doped with Pr^{3+}. Depending on the crystal field, Pr^{3+} can exhibit both *d-f* and *f-f* types of emission. *d-f* emission is usually faster than that of Ce, whereas *f-f* is slower. Pr^{3+} doping level of 1% (on molar basis) was explored in our research. Scintillation properties such as emission spectrum, decay time spectrum and light output of $LaBr_3$:Pr were measured.

Emission spectrum of $LaBr_3$:Pr was measured upon excitation of the sample with X-rays using the approach described earlier. The resulting emission spectrum for $LaBr_3$:Pr is shown in **Figure 21**. The spectrum indicates that the emission arising from *5d-4f* transition of Pr^{3+} is absent in the sample. Spectroscopic measurements indicate that this may be because the charge transfer from the valence band to Pr^{3+} occurs at energies below that required for *5d-4f* emission. However, there is efficient energy transfer from the host to the activator ions leading to strong emission from $4f^2$-$4f^2$ transition of Pr^{3+}. Multiple transitions associated with Pr^{3+} lead to a rather complicated and rich spectrum which is predominantly in the red-region. This red-emission of $LaBr_3$:Pr is interesting because it is well matched to the optical response of silicon photodiodes.

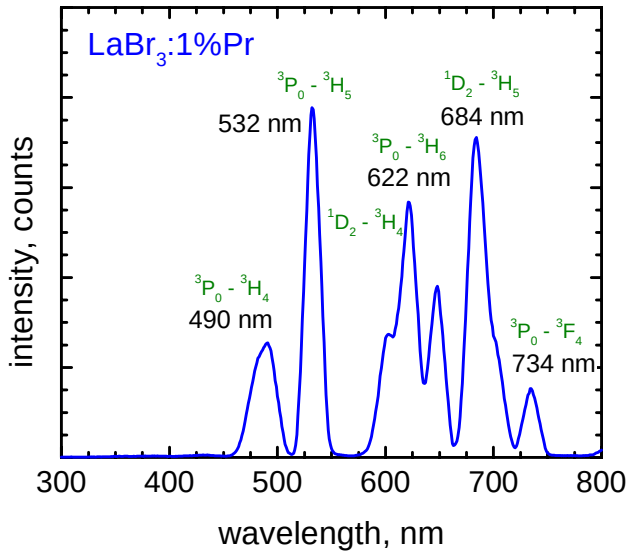

Figure 21. X-ray induced emission spectrum for $LaBr_3$:Pr. Various transitions corresponding to observed peaks in the emission spectrum are also shown.

The temporal response of $LaBr_3$:Pr sample was measured using delayed coincidence method [Bollinger] and the result is shown in **Figure 22**. From an exponential fit to the temporal response, the decay time constant was estimated to be ~11 μs. Since much of the emission for $LaBr_3$:Pr originates from ^3P_o level (see **Figure 21**), the lifetime of this level governs the decay time constant for $LaBr_3$:Pr. The calculated lifetime for ^3P_o level in $LaCl_3$:Pr based on Judd-Ofelt theory is ~12.5 μs [Gatch], which is in reasonable agreement with our measured decay time constant for $LaBr_3$:Pr. Due to cross-relaxation, the decay time of Pr emission should depend on the activator concentration. For example crystal of Y_2O_3 doped with different Pr concentrations shows such an attenuation of decay time constant. For Y_2O_3:Pr, the decay time decreases from 124 μs to 4 μs

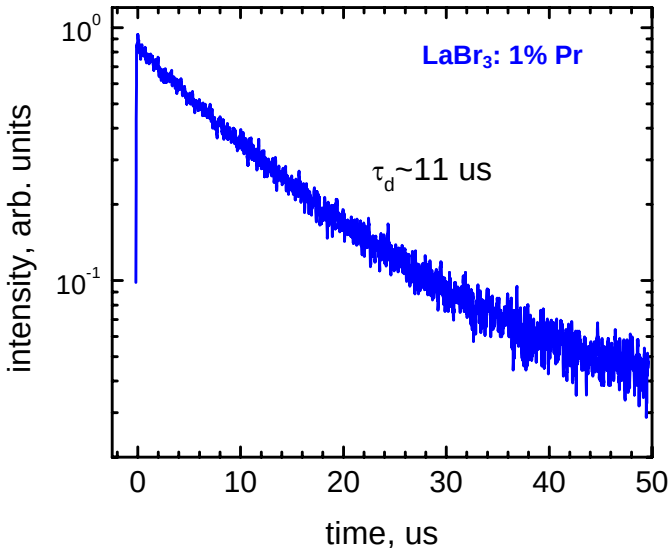

Figure 22. Gamma-ray induced decay time spectrum for a $LaBr_3$ sample doped with 1% Pr^{3+}.

as the Pr^{3+} concentration is increased from 0.1% to 2.5% [Guyot]. Initial results in Phase I research at RMD also indicate that such a trend exists for $LaBr_3$:Pr. By increasing the Pr^{3+} concentration to 5% in $LaBr_3$, the decay time constant was found to be ~5 μs. We will explore a wider range of Pr^{3+} concentration in $LaBr_3$ in the Phase II research.

Light output of $LaBr_3$ sample with 1% Pr doping has also been measured in the Phase I research. In view of the red-emission of the $LaBr_3$:Pr sample, the light output measurements were performed with RMD's silicon avalanche photodiodes (APD) [Shah 01]. These APDs operate with high gain (>1000), low noise (<100 electrons-rms) and high quantum efficiency (~60% at λ≥500 nm). Since these silicon APDs can also detect low energy X-rays directly, an ^{55}Fe spectrum (5.9 keV X-rays) was recorded first (without any scintillator) to allow calibration of the energy scale. ^{137}Cs spectrum was recorded using a $LaBr_3$:Pr crystal (wrapped in Teflon) coupled to the same APD (see **Figure 23a**). Based on the position of the 662 keV photopeak (in comparison to the directly detected 5.9 keV X-ray peak), the APD quantum efficiency, the known silicon conversion efficiency of 3.6 eV (to create an electron-hole pair upon X-ray interaction), and scintillator-APD coupling efficiency, the light yield of the $LaBr_3$:Pr sample was estimated to be 85,000 photons/MeV, which is ~15% higher than the light yield of $LaBr_3$ doped with Ce. This is the highest light yield for a scintillator that emits in red-region. Upon optimization of the test setup, the energy resolution of the 662 keV photopeak was measured to be ~4% (FWHM) in this study (see **Figure 23b**), which is promising. Proportionality of response for $LaBr_3$:Pr was very good. Over 60 keV to 1 MeV γ-ray energy range, its non-proportionality was ~4%.

Thus, $LaBr_3$:Pr appears to be a very interesting scintillator. Particularly attractive features of this material are its high light output and red-emission, which would make it an excellent match for silicon photodiode based systems. While its

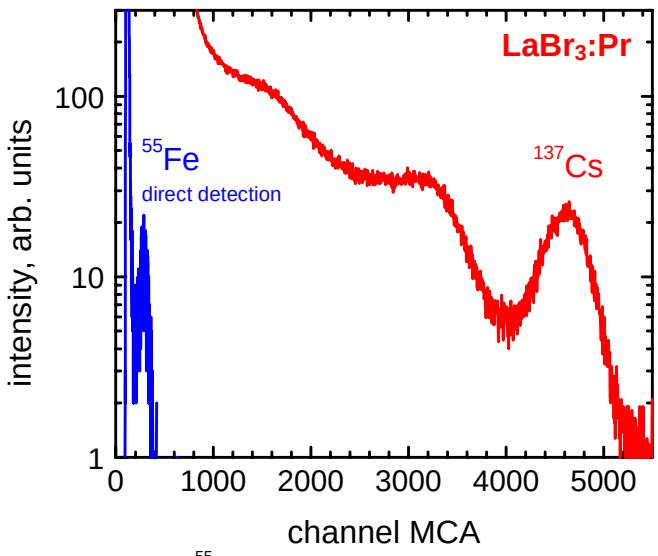

Figure 23a. ^{55}Fe spectrum (5.9 keV x-rays) detected directly with a silicon APD (in blue) and ^{137}Cs spectrum with same APD coupled to a $LaBr_3$:Pr crystal (in red). From the calibration provided by the 5.9 keV peak, the light output of $LaBr_3$:Pr crystal was estimated to be 85,000 photons/MeV.

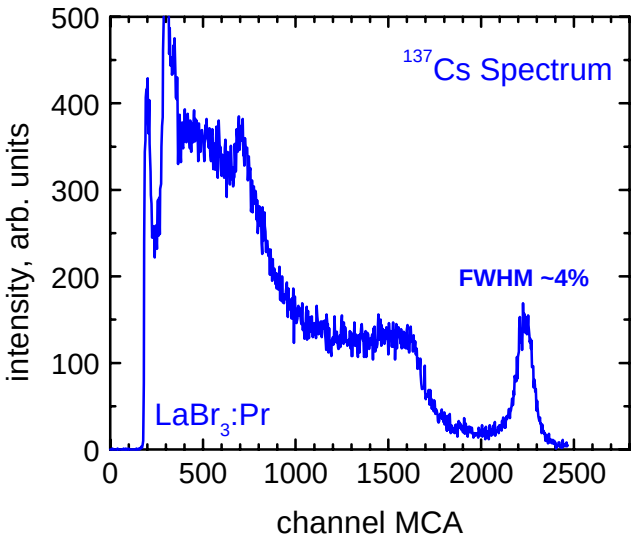

Figure 23b. ^{137}Cs spectrum recorded with $LaBr_3$ crystal (1% Pr doping) to a Si APD. The energy resolution of the 662 keV peak is ~4% (FWHM).

response is slow compared to Ce^{3+} doping, for many applications its speed is fast enough. Further improvement in speed, light output and energy resolution of $LaBr_3$:Pr should be possible upon optimization of the crystal quality and its doping level. These issues will be explored in the Phase II research. The scintillation properties of $LaBr_3$:Pr crystals are summarized in **Table 1** along with those for other crystal compositions investigated in the Phase I research at the end of this final report. A discussion of performance of lanthanum and cerium bromide crystals at high temperatures is provided in the following section.

G. Performance of $LaBr_3$:Ce and $CeBr_3$ at High Temperature

In a related research effort, we have investigated performance of $LaBr_3$:Ce and $CeBr_3$ at elevated temperatures for use in oil well logging instrumentation. Since the ability to perform at high temperatures may be relevant in some nuclear waste clean-up activities, the high temperature performance of $LaBr_3$:Ce and $CeBr_3$ crystals is discussed here. In order to conduct these measurements, a custom designed oven for elevating and maintaining the temperature of both photomultiplier tube (Hamamatsu R4607-01) and scintillator was built at RMD. Using such a setup, the light output and decay time of $LaBr_3$ (0.5% Ce) and $CeBr_3$ crystals were measured in 25 to 175 °C temperature range.

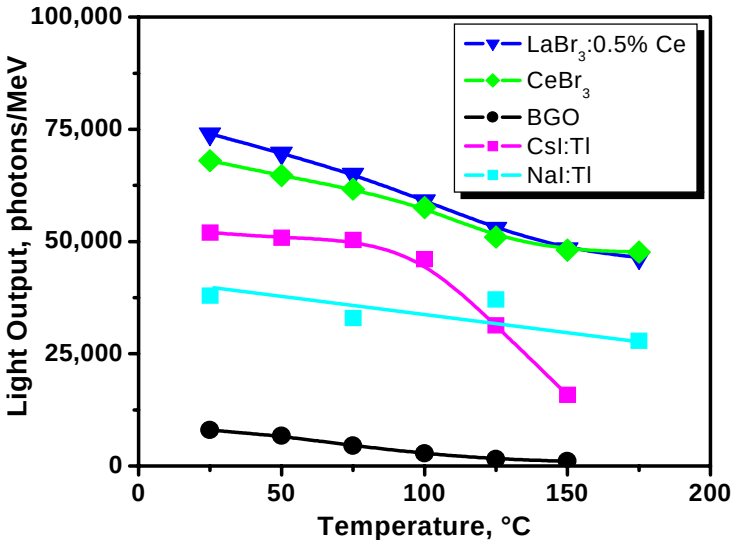

Figure 24. Variation in light yield as a function of temperature for various scintillators including $LaBr_3$:Ce and $CeBr_3$.

Figure 24 shows the variation in light yield of $LaBr_3$:Ce and $CeBr_3$ scintillators as a function of temperature. Also shown in the same figure are the results for established scintillators such as BGO, NaI:Tl and CsI:Tl that were measured using the same experimental setup. The high temperature results are very encouraging and indicate that $LaBr_3$:Ce and $CeBr_3$ show high light yield at elevated temperature. For example, at 175 °C, the light yield of $LaBr_3$:Ce and $CeBr_3$ is up to 80% higher than that for NaI:Tl. Furthermore, at elevated temperature (>100 °C), the light yield of $LaBr_3$:Ce and $CeBr_3$ is more than an order of magnitude higher than that for BGO.

Variation of the principal decay time constant as a function of temperature for $LaBr_3$:Ce, $CeBr_3$ and NaI:Tl is shown in **Figure 25**. As seen in the figure, $LaBr_3$:Ce and $CeBr_3$ show fast response with principal decay time constant less than 30 ns at 175 °C for both materials. Thus, $LaBr_3$:Ce and $CeBr_3$ would provide high count-rates at elevated temperatures. The decay time constant for NaI:Tl is longer, and is about 90 ns at 175 °C.

Initial investigation of proportionality of response of these cerium based rare earth halide scintillation materials at 175 °C has also been carried out and the results indicate that over 100 keV to 1 MeV gamma-ray energy range, the non-proportionality is as low as 5%. This is very encouraging because it indicates that these materials should provide excellent energy resolution at high temperatures. In fact, we have already confirmed that at 100 °C, the energy resolution of these rare earth halide scintillators is comparable to their room temperature value. Some degradation in energy resolution at even higher temperatures was observed, mostly due to the drop in the quantum efficiency of the PMT used at elevated temperatures. However, in our measurements in the 125 to 175 °C temperature range using ^{137}Cs source (662 keV photons), the energy resolution achieved with $CeBr_3$ and $LaBr_3$:Ce was ~3.5 times better than that for CsI:Tl, >9 times better than that for BGO and ~2 times better than that for NaI:Tl, which is very encouraging. Thus, these new scintillators appear to be promising for nuclear waste clean-up applications that require high temperature operation.

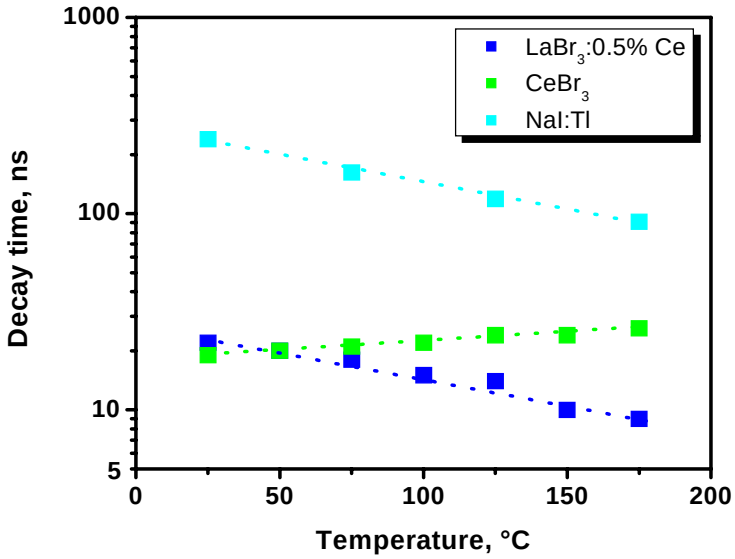

Figure 25. Variation of the principal decay time constant of $LaBr_3$:Ce, $CeBr_3$ and NaI:Tl versus temperature.

H. SUMMARY

The goal of the Phase I research was to investigate lanthanum halide and related scintillators for nuclear waste clean-up. A number of compositions were investigated in the Phase I research and a summary of their scintillation properties is provided in **Table 1**. Properties of NaI:Tl are also listed in **Table 1** for comparison. In the table, more than one decay component is listed only when the faster component does not cover more than 50% of the emitted light. As seen in the table, $LaBr_3$:Ce remains a very promising scintillator with high light yield and fast response. $CeBr_3$ is attractive because it is very similar to $LaBr_3$:Ce in terms of scintillation properties and also has the advantage of much lower self-radioactivity, which may be important in some applications. $CeBr_3$ also shows slightly higher light yield at higher temperatures than $LaBr_3$ and may be easier to produce with high uniformity in large volume since it does not require any dopants.

Among the mixed lanthanum halides, the light yield of $LaBr_xI_{3-x}$:Ce is lower and the difference in crystal structure of the binaries ($LaBr_3$ and LaI_3) makes it difficult to grow high quality crystals of the ternary as the iodine concentration is increased. On the other hand, $LaBr_xCl_{3-x}$:Ce provides excellent performance. Its light output is high and it provides fast response. The crystal structure of the two binaries ($LaBr_3$ and $LaCl_3$) is very similar. Overall, its scintillation properties are very similar to those for $LaBr_3$:Ce. While the gamma-ray stopping efficiency of $LaBr_xCl_{3-x}$:Ce is lower than that for $LaBr_3$:Ce (primarily because the density of $LaCl_3$ is lower than that of $LaBr_3$), it may be easier to grow large crystals of $LaBr_xCl_{3-x}$:Ce (than

$LaBr_3$:Ce) since in some instances (for example, $Cd_xZn_{1-x}Te$), the ternary compounds provide increased flexibility in the crystal lattice.

Table 1. Properties of Scintillators Investigated in the Phase I Research

Material	Light Output [Photons/ MeV]	Wavelength of Maximum Emission [nm]	Decay Lifetimes [ns]	Attenuation Length (511 keV) [cm]
NaI(Tl)	38,000	415	230	3.0
$LaBr_3$ (0.5% Ce)	74,000	370	26	2.1
$CeBr_3$	68,000	370	17	2.1
$LaBr_{2.4}I_{0.6}$ (0.5% Ce)	30,000	450	33, 360	1.9
$LaBr_{1.5}Cl_{1.5}$ (10% Ce)	68,000	380	20	2.4
$LaBr_3$ (1% Eu^{2+})	10,000	430	90, 560	2.1
$LaBr_3$ (1% Pr^{3+})	85,000	610*	11,000	2.1

* - weighted mean

Among the new dopants, Eu^{2+} and Pr^{3+}, tried in $LaBr_3$ host crystals, the Eu^{2+} doped samples exhibited low light output. This was mostly because a large fraction of light was emitted via very slow decay components (>50 μs) and as a result was not included in the light estimation performed using gamma-ray spectroscopy where the typical amplifier integration time used is ≤12 μs. The origin of these slow component(s) is most likely related to the presence of defects caused by charge imbalance in the crystals. The charge imbalance occurs when the Eu^{2+} ions replace the La^{3+} ions in crystal lattice. This charge neutrality can be restored by codoping the Eu^{2+} doped $LaBr_3$ crystals with ions such as Hf^{4+}. The Pr^{3+} doped $LaBr_3$ crystals provided exciting results. They exhibited very high light yield (85,000 photons/MeV) and good energy resolution. While the decay time of $LaBr_3$:Pr is much slower than that for $LaBr_3$:Ce, it is fast enough for many nuclear waste cleanup applications. Furthermore, it should be possible to increase the speed of $LaBr_3$:Pr by adjusting its Pr^{3+} concentration. The most exciting feature of $LaBr_3$:Pr is that it emits in red-region and is therefore, well suited for silicon photodiode readout. In fact, $LaBr_3$:Pr is the brightest scintillator in the red-region and its light yield is ~15% higher than the light yield of $LaBr_3$ doped with Ce.

Overall, the Phase I research has been very successful and has lead to better understanding of the lanthanum halide and related scintillators. It has also opened up some promising avenues to optimize the performance of these exciting scintillators. Based on the Phase I results, we have clearly demonstrated the feasibility of the proposed approach.

I. LITERATURE CITED

H. H. Barrett, J. D. Eskin, and H.B. Barber, *Charge Transport in Arrays of Semiconductor Gamma-Ray Detectors*, Physical Review Letters, Vol. **75 (1)**, p. 156, (1995).

A.Bessiere: *Luminescence and scintillation properties of the small band gap compound* $LaI_3:Ce^{3+}$, presented at SCINT 2003, Valencia, Spain, September, 2003.

L. M. Bollinger and G. E. Thomas, *Measurement of the time dependence of scintillation intensity by a delayed-coincidence method*, Rev Sci Instr, vol. 32, pp. 1044, (1961).

S.R. Bowman et. al., *A 7-μm Praseodymium-Based Solid State Laser*, IEEE J. of Quantum Electronics, V.32(4), (1996).

J.C. Brice, **Crystal Growth Processes**, Blackie Halsted Press, (1986).

K. Burr, J. LeBlanc, S. Zelakiewicz, A. Ganin, C. L. Kim, D. L. McDaniel, K. S. Shah, R. Grazioso, R. Farrell, J. Glodo, *Evaluation of Position Sensitive Avalanche Photodiodes for PET*, presented at IEEE Nuc. Sci. Symp., Norfolk, VA, Nov. (2002).

Byrnes, **Field Sampling Methods for Remedial Investigation**, Lewis Publishers, (1994).

P. Dorenbos, "*Energy of the first* $4f^7 \rightarrow 4f^6 5d$ *transition of* Eu^{2+} *in inorganic compounds*," J. Lum., vol. 104, pp. 239-260, (2003).

P. Dorenbos, *Light output and energy resolution of* Ce^{3+} *doped scintillators*, *Nucl. Instr. and Meth.*, pp. (submitted for publication), 2001.

P. Dorenbos, *et. al.*, *Non-Proportionality in the Scintillation Response and the Energy Resolution Obtainable with Scintillation Crystals*, IEEE Trans. Nuc. Sci., 42, 2190, (1995).

D. B. Gatch, W. M. Dennis, W. M. Yen, "*Photon avalanche effect in* $LaCl_3:Pr^{3+}$", Physical Review B, 62, 10790-10796, (2000).

E.L. Gershey, R.C. Klein, E. Party, A. Wilkerson, **Low Level Radioactive Waste**, Von Nostrand Reinhold, (1990).

J. Glodo, W.W. Moses, W.M. Higgins, E.V.D. van Loef, P. Wong, S.E. Derenzo, M.J. Weber, and K.S. Shah, *Effects of Ce Concentration on Scintillation Properties of* $LaBr_3:Ce$, Presented at IEEE Nuc. Sci. Symp., Rome, Oct. (2004), submitted for publication in IEEE NSS/MIC/RTSD Conference Record.

B. C. Grabmaier, W. Rossner, T. Berthold, *Proc. Intl. Conf. on Inorganic Scintillators, SCINT95*, Delft University Press, The Netherlands, 1996.

O. Guillot-Noel et al., *Scintillation Properties of* $RbGd_2Br_7:Ce$ *Advantages and Limitations*, IEEE Trans. Nuc. Sci., V46(5), (1999).

Y. Guyot, R. Moncorge, L. D. Merkle, A. Pinto, B. McIntosh, H. Verdun, *"Luminescence properties of* Y_2O_3 *single crystals doped with* Pr^{3+} *or* Tm^{3+} *and codoped with* Yb^{3+}, Tb^{3+} *or* Ho^{3+} *ions"*, Optical Materials 5, 127-136, (1996).

He, Zhong, *Potential distribution within semiconductor detectors using coplanar electrodes*, NIM A, **Vol 365**, 572-575, (1995).

K.J. Hofstetter, *Environment Radiation Monitoring Technology: Capabilities and Needs*, Nucl. Inst. and Meth., A 353, p. 472, (1994).

G. Knoll, **Radiation Detection and Measurement**, 3rd Ed., John Wiley and Sons, (1999).

P.N. Luke, *Unipolar Charge Sensing with Coplanar Electrodes-Application to Semiconductor Detectors*, IEEE Trans. Nuc. Sci., **V.42(4)**, p. 207, (1995).

J.E. Meisner, W.F. Nicaise and D.C. Stromswold, *CsI(Tl) with Photodiode for Identifying Subsurface Radionuclide Contamination*, IEEE Trans. Nuc. Sci., 42(4), (1995).

W. Mengesha, T. D. Taulbee, B. D. Rooney, et al., *Light yield nonproportionality of CsI(Tl), CsI(Na), and YAP*, IEEE Trans. Nucl. Sci., vol. 45, pp. 456-461, 1998.

Moses WW, Current Trends in Scintillator Detectors and Materials, accepted for publication in Nucl. Inst. And Meth., (2001).

OTA: U.S. Congress, Office of Technology Assessment, *Complex Cleanup, The Environment Legacy of Nuclear Weapons Production*, OTA-O-484, Washington, DC: U.S. Government Printing Office, (1991).

V. Radeka, *Low-Noise Techniques in Detectors*, Ann. Rev. Nucl. Part. Sci., **38**, p. 217, (1988).

R. Redus, R. Farrell, *Gain and Noise in Avalanche Photodiodes: Theory and Experiment*, for submission to SPIE Proc. (1995).

P. A. Rodnyi, **Physical Processes in Inorganic Scintillators**, CRC Press, New York, (1997)

T.E. Schlesinger and R.B. James, editors, **Semiconductors for Room Temperature Nuclear Detector Applications**, New York: Academic Press, 1995.

K.S. Shah, J. Glodo, W.W. Moses, S.E. Derenzo, M.J. Weber, "$LaBr_3$:Ce Scintillators for γ-Ray Spectroscopy," *IEEE Trans. Nuc. Sci.*, V50(6), p. 2410, (2003).

K.S. Shah, J. Glodo, M. Klugerman, W. Higgins, and P. Wong, *High Energy Resolution Scintillation Spectrometers*, presented at IEEE RTSD/NSS/MIC, Portland, October (2003b).

K.S. Shah, R. Farrell, R. Grazioso, E. Harmon, and E. Karplus, *Position-Sensitive Avalanche Phtotodiodes for Gamma-Ray Imaging*, IEEE Transactions on Nucl. Sci., Vol. **49**, August (2002).

K.S. Shah, R. Farrell et al., *Large Area APDs and Monolithic APD Arrays*, IEEE Trans. Nuc. Sci., V. 48(6), p. 2352 (2001).

Squillante, M.R.; Cirignano, L.; Grazioso, R. *Room Temperature Semiconductor Device and Array Configurations*, Presented at E-MRS Vienna Conference, France, October 11-15, 1999.

C.W.E. van Ejik, *New inorganic scintillators – aspects of energy resolution*, Nuc. Inst. and Meth. in Phys. Res. A 471 pp.244-248, (2001).

E.V.D. van Loef, P. Dorenbos, C.W.E. van Ejik, K. Kramer, and H.U. Gudel, *High Energy Resolution Scintillator: Ce^{3+} Activated $LaBr_3$*, Appl. Phys. Lett., 79(10), p.1573, (2001a).

E.V.D. van Loef, P. Dorenbos, and C.W.E. van Ejik, K. Kramer, and H.U. Gudel, *Scintillation properties of $LaBr_3$:Ce^{3+} crystals: Fast, Efficient and High-energy-resolution Scintillators*, Presented at SCINT 2001, Chamonix, France, September (2001b).

E.V.D. van Loef, P. Dorenbos, C.W.E. van Ejik, K. Kramer, and H.U. Gudel, *High Energy Resolution Scintillator: Ce^{3+} Activated $LaCl_3$*, Appl. Phys. Lett., 77(10), p.1467, (2000a).

M. Woodring, G.Entine et al., *Advanced radiation imaging of low-intensity gamma ray sources*, Nuc. Inst. and Meth. in Phys. Res., A422, p. 709, (1999).